

Dynamics of a period-three pattern loaded Bose-Einstein condensate in an optical lattice

A.-M. Rey^{1,2}, P. B. Blakie², and Charles W. Clark²

¹*Institute for Physical Science and Technology, University of Maryland, College Park, MD 20742 and*

²*Electron and Optical Physics Division, National Institute of Standards and Technology,
Technology Administration, U.S. Department of Commerce, Gaithersburg, MD 20899-8410*

(Dated: November 16, 2018)

We discuss the dynamics of a Bose-Einstein condensate initially loaded into every third site of an optical lattice using a description based upon the discrete nonlinear Schrödinger equation. An analytic solution is developed for the case of a periodic initial condition and is compared with numerical simulations for more general initial configurations. We show that mean field effects in this system can cause macroscopic quantum self-trapping, a phenomenon already predicted for double well systems. In the presence of a uniform external potential, the atoms exhibit generalized Bloch oscillations which can be interpreted in terms of the interference of three different Bloch states. We also discuss how the momentum distribution of the system can be used as experimental signature of the macroscopic self trapping effect.

PACS numbers: 03.75.F, 05.30.Jp

I. INTRODUCTION

An optical lattice is a periodic potential formed by the Starkshift at the intersection region of two far detuned laser fields. A Bose-Einstein condensate loaded into such an optical lattice is a useful system for studying and controlling the dynamics of ultra-cold atoms. In this system experimental studies in the meanfield regime have provided elegant demonstrations of band structure [1, 2, 3] and quantum chaos [4], and have considered the effects of nonlinearity on the condensate dynamics [5, 6, 7]. By suitably loading a condensate into deep optical lattices, number squeezing [8] and the Mott-Insulator transition [9] have been observed.

In this paper, we investigate a Bose-Einstein condensate loaded into every third site of an optical lattice, motivated by the recent experimental realization of this system by the NIST group [10]. In that experiment a combination of two independently controlled lattices was used to prepare the condensate into every third site of a single lattice. Briefly the procedure consists of loading a condensate into the ground band of lattice with periodicity $3a$, so that the condensate is well localized in the potential minima of this lattice. A second lattice of periodicity a which is parallel to the first lattice, is then ramped up so that the superimposed light potentials form a *super-lattice* of period $3a$. For the ideal case both lattice potentials are in-phase, and the addition of the second lattice will not shift the locations of the potential minima from those of the first lattice alone and the condensate will remain localized at these positions. Finally, by removing the first period- $3a$ lattice on a time scale long compared to band excitations, but short compared to the characteristic time of transport within the lattice, the condensate will be left in every third site of the period- a lattice.

A condensate loaded in this way is not an eigenstate of the final period- a lattice, and the condensate will continue to evolve in the final system. Outside the strongly correlated regime (where the depletion becomes large [11]) the Gross-Pitaevskii equation is expected to give a good description of the condensate dynamics, and has been applied to the lattice system [12, 13]. In our system we assume the lattice is suf-

ficiently deep that a tight binding description is applicable, and the Gross-Pitaevskii equation can be reduced to a discrete nonlinear Schrödinger equation involving only an onsite nonlinear interaction and nearest neighbor tunneling. For the periodic initial condition of equal wavefunction amplitude every third site and zero at all others, symmetry arguments can be used to reduce the wavefunction evolution to a two mode problem (analogous to a double well system with an energy offset) for which an analytic solution of the dynamics can be given. We show that for large ratios of the interatomic interaction strength to tunneling energy the condensate evolves with self-maintained population imbalance, whereby the condensate population tends to remain localized in the initially occupied lattice sites. A similar phenomenon has been studied in double wells systems [14, 15, 16, 17, 18]. We show that the momentum distribution of an interacting condensate changes in time in a manner which can be related to the spatial tunneling of condensate, and would be a suitable experimental observable.

Under the influence of an external force a Bloch state will accelerate until it reaches the zone edge where it will Bragg scatter to the opposite side of the Brillouin zone. This periodic motion, known as Bloch oscillations, has been observed in systems of cold atoms [19] and Bose-Einstein condensates in optical lattices [3, 5]. To illustrate how a linear potential affects the motion of a pattern loaded condensate we find analytic solutions for the noninteracting case with periodic initial condition and show how the dynamics for this system can be interpreted in terms of the interference of three Bloch states of the lowest band Bloch oscillating in unison. We present numerical results for more general (non-periodic) initial conditions and consider characteristic properties of the momentum distribution.

In Section II we start by reviewing the basic formalism of a Bose-Einstein condensate in an optical lattice in the tight binding approximation. In Section III we study the dynamics for the case when only the optical potential is present. We discuss a periodic model and compare its predictions with numerical simulations for more general initial conditions. In section IV we consider the dynamics of a Bose-Einstein condensate in

the lattice with the presence of constant external force.

II. TIGHT BINDING DESCRIPTION OF A BEC IN AN OPTICAL LATTICE

The dynamics of a condensate in the lattice can be modelled by the 1D Gross-Pitaevskii equation

$$i\hbar \frac{\partial \Phi}{\partial t} = -\frac{\hbar^2}{2M} \frac{\partial^2 \Phi}{\partial x^2} + V_0 \sin^2 \left(\frac{2\pi}{\lambda} x \right) \Phi + V_{\text{Ext}}(x) \Phi + N \frac{4\pi\hbar^2 a_1}{M} |\Phi|^2 \Phi, \quad (1)$$

where $V_{\text{Ext}}(x)$ is the external potential, V_0 is the depth of the optical potential which is determined by the intensity of the laser beams, λ is the wavelength of the lasers, a_1 is the 1D renormalized scattering length with dimension of an inverse length (which we obtain by requiring that the value of the chemical potential for the 3D system matches the 1D chemical potential [20], M is the atomic mass and N the total number of atoms.

In the tight-binding approximation, valid if the height of the lattice is higher than the chemical potential at each well, the 1D condensate order parameter can be expanded in a Wannier basis keeping only the lowest band [21]:

$$\Phi(x, t) = \sum_n \Psi_n(t) \phi_n(x), \quad (2)$$

where $\phi_n(x) = \phi(x - na)$ is the condensate Wannier function centered on the n^{th} lattice site, with $\int dx \phi_n(x) \phi_{n+1}^*(x) = 0$ and $\int dx |\phi_n(x)|^2 = 1$, $a = \lambda/2$ is the lattice constant, and $\Psi_n(t)$ is the n^{th} amplitude. Replacing this ansatz in Eq. 1, the Gross-Pitaevskii equation reduces to the discrete nonlinear Schrödinger equation and the Ψ_n satisfy:

$$i\hbar \frac{\partial \Psi_n}{\partial t} = -J(\Psi_{n-1} + \Psi_{n+1}) + (\epsilon_n + NU|\Psi_n|^2)\Psi_n, \quad (3)$$

where $U = (4\pi\hbar^2 a_1/M) \int dx |\phi_n|^4$ is the strength of the on-site repulsion of two atoms occupying the lattice site n , $\epsilon_n = \int V_{\text{Ext}}(x) |\phi_n|^2 dx$ describes the energy offset of each lattice site n , and $J = \int \phi_{n+1}^* [-(\hbar^2/2M)(\partial^2/\partial x^2) + V_0 \sin^2(2\pi x/\lambda)] \phi_n dx$ is the hopping matrix element between adjacent sites. As shown in Ref. [22, 23], Eq. (3) can be seen as an equation of motion $i\hbar \partial \Psi_n / \partial t = \partial H / \partial \Psi_n^*$, derived from a Hamiltonian function H given by

$$H = \sum_n -J (\Psi_n^* \Psi_{n+1} + \Psi_{n+1}^* \Psi_n) + \epsilon_n |\Psi_n|^2 + \frac{NU}{2} |\Psi_n|^4, \quad (4)$$

with $i\Psi_n^*$ and Ψ_n treated as canonically conjugate variables. Both the Hamiltonian H and the norm $\sum_n |\Psi_n|^2 = 1$ are conserved quantities.

The major interest of this paper is in the tunneling properties of the condensate in the lattice, and in the noninteracting

case the time scale for tunneling is determined by the hopping matrix element J . For this reason it is convenient to define a new scale of time $\tau = Jt/\hbar$, and energies $E_n = \epsilon_n/J$ and coupling constant $\Lambda = NU/J$. In terms of these new variables the tight binding evolution equation (3) takes the form

$$i \frac{\partial \Psi_n}{\partial \tau} = -(\Psi_{n-1} + \Psi_{n+1}) + (E_n + \Lambda |\Psi_n|^2) \Psi_n, \quad (5)$$

III. CASE OF NO EXTERNAL POTENTIAL

A. The case of periodic initial conditions: reduction to a two mode system

The stationary states and other aspects of the dynamics of Eq. (5) have been discussed by others previously [22, 23, 24]. We are motivated by recent experiments to treat the case of the particular nonstationary state described in the introduction, in which a condensate is initially loaded into every third site of an optical lattice. We treat first a model case in which no external potential is present, ($E_n = 0$), and in which the initial occupancies of each third site are the same, and in which the condensate initially has a uniform phase. At $\tau = 0$, the amplitudes $\Psi_n(\tau)$ are given by

$$\Psi_{3n}(0) = \sqrt{\rho}, \quad (6)$$

$$\Psi_{3n+1}(0) = \Psi_{3n+2}(0) = 0, \quad (7)$$

where $N\rho$ is the initial number of atoms per occupied site. This initial condition is homogeneous in the sense that each occupied site has the same amplitude and phase along the length of the lattice. For an infinite lattice, or one with periodic boundary conditions, the amplitudes for all initially occupied sites (Ψ_{3n}) evolve identically in time, and the amplitudes for the initially unoccupied sites satisfy $\Psi_{3n+1}(\tau) = \Psi_{3n+2}(\tau)$ for all τ and all n . This allows us to reduce the full set of equations (5) to a set of two coupled equations

$$i \frac{\partial \Psi_0}{\partial \tau} = -2\Psi_1 + \Lambda |\Psi_0|^2 \Psi_0, \quad (8)$$

$$i \frac{\partial \Psi_1}{\partial \tau} = -(\Psi_1 + \Psi_0) + \Lambda |\Psi_1|^2 \Psi_1, \quad (9)$$

where $\Psi_{3n} \equiv \Psi_0$ and $\Psi_{3n+1} = \Psi_{3n+2} \equiv \Psi_1$ for all n . The normalization condition is

$$|\Psi_0|^2 + 2|\Psi_1|^2 = \rho. \quad (10)$$

The Hamiltonian function, H , of this system is (from Eq. 4)

$$\begin{aligned} H &= \frac{J}{\rho} \left(-2(\Psi_0^* \Psi_1 + \Psi_0 \Psi_1^*) - 2|\Psi_1|^2 + \frac{\Lambda}{2} |\Psi_0|^4 \right. \\ &\quad \left. + \Lambda |\Psi_1|^4 \right) \\ &= \frac{J\Lambda\rho}{2}. \end{aligned} \quad (11)$$

By writing $\Psi_0 = \psi_0 \sqrt{\rho}$ and $\Psi_1 = \psi_1 \sqrt{\rho/2}$, we can transform Eqs. (8)-(9) to the form

$$i \frac{\partial}{\partial \tau} \begin{pmatrix} \psi_0 \\ \psi_1 \end{pmatrix} = \begin{pmatrix} \gamma |\psi_0|^2 & -\sqrt{2} \\ -\sqrt{2} & \gamma \frac{|\psi_1|^2}{\sqrt{2}} - 1 \end{pmatrix} \begin{pmatrix} \psi_0 \\ \psi_1 \end{pmatrix}, \quad (12)$$

where $\gamma = \Lambda \rho$ is the ratio of on-site repulsion to tunneling energies, and the normalization condition (10) is now $|\psi_0|^2 + |\psi_1|^2 = 1$. The factor of $\sqrt{2}$ difference in the definition of ψ_0 and ψ_1 arises because ψ_1 represents the amplitude of the two initially unoccupied sites. With this factor incorporated, the matrix appearing in Eq. (12) is explicitly Hermitian. We note this equation of motion is identical to that for a condensate in a double well trap in the two mode approximation [25, 26].

We note in passing that a similar reduction, to a system of $[m/2] + 1$ equations, exists for lattice systems that are loaded such that only every m -th site is initially occupied.

B. Solution of the equations of motion

It is convenient to write the lattice site amplitudes appearing in Eqs. (8) and (9) as $\Psi_0 = f e^{i\theta_0} \sqrt{\rho}$ and $\Psi_1 = g e^{i\theta_1} \sqrt{\rho}$, where f, g , and θ are real. By introducing the phase difference $\phi = \theta_0 - \theta_1$, Eqs. (8), (9) and (11) can be recast as

$$\dot{f} = 2g \sin \phi, \quad (13)$$

$$\dot{g} = -f \sin \phi, \quad (14)$$

$$\frac{\gamma}{2} = -4fg \cos \phi + \frac{\gamma}{2} (f^4 + 2g^4) - 2g^2, \quad (15)$$

The analytic solutions of Eqs. (13)-(15), found using a procedure similar to that presented by Raghavan *et al.* [14], can be expressed in terms of Weierstrassian elliptic functions $\wp(\tau; g_2, g_3)$ [27]. The analytic solutions are

$$f(\tau) = \sqrt{1 - \frac{24}{12\wp(\tau; g_2, g_3) + (9 + 2\gamma + \gamma^2)}}, \quad (16)$$

$$g(\tau) = \sqrt{\frac{1 - f(\tau)^2}{2}}, \quad (17)$$

where the parameters g_2 and g_3 are given by

$$g_2 = (81 - 14\gamma^2 + 4\gamma^3 + \gamma^4) / 12, \quad (18)$$

$$g_3 = (729 + 243\gamma^2 - 46\gamma^3 - 15\gamma^4 + \gamma^6) / 216. \quad (19)$$

The solutions $f(\tau)$ and $g(\tau)$ are oscillatory functions whose amplitudes and common period, $T(\gamma)$, are determined by the parameter γ (see Figs. 1 and 2). It is useful to qualitatively divide this behavior into two regimes, separated by $\gamma = 2$. Analysis of Eqs. (13) - (15) shows that $f(\tau_0) = g(\tau_0)$ for some value of τ_0 when $\gamma \leq 2$, and for $\gamma > 2$, $f(\tau) > g(\tau)$ for all τ .

1. The tunneling dominated regime

For $\gamma \lesssim 2$, we find that the oscillation period is essentially constant (see Fig. 1).

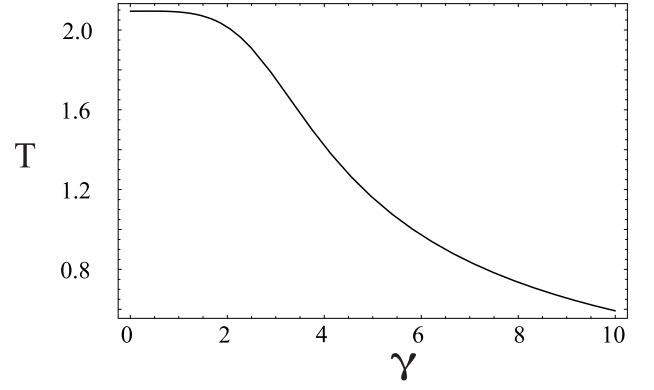


FIG. 1: Oscillation period (in units of \hbar/J) as a function of the interaction strength γ .

In this case the role of interactions is relatively small, and the behavior can be approximately understood by taking $\gamma = 0$, in which case the matrix of Eq. (12) is constant in time. The equations of motion in this case are equivalent to those of a two-state Rabi problem [28], where the two levels are coupled by a Rabi frequency of strength $\sqrt{2}$, which is detuned from resonance by -1 . This system will undergo Rabi oscillations whereby atoms periodically tunnel from the initially occupied site into the two neighboring sites. Because the coupling is detuned from resonance the transfer of populations between wells is incomplete, with $|\psi_1|^2$ attaining a maximum value of $8/9$. The Rabi model predicts that the cycling frequency between the levels is equal to the difference between the eigenvalues of the matrix of matrix of Eq. (12), which gives the period of oscillation as $T_{\text{Rabi}} = 2\pi/3$ in units of \hbar/J (see Fig. 1).

2. Interaction dominated regime

The effect of interactions on the mean-field dynamics is to cause the energies of the initially occupied sites to shift relative to those of the unoccupied sites. As γ increases and this energy shift increases relative to the strength of coupling between sites, the tunneling between sites occurs at a higher frequency, but with reduced amplitude. The population of the initially occupied sites becomes self trapped by the purely repulsive pair interaction, which in the context of a double well system has been called “macroscopic quantum self trapping” [26]. This is demonstrated quantitatively in Fig. 2 where we plot the minimum value of f^2 occurring during the oscillation as a function of γ . In contrast to the tunneling dominated regime, where tunneling periodically populates all sites equally, the condensate tends to be localized on the initially occupied sites in the interaction-dominated regime.

C. Momentum space dynamics

Typically the spacing between individual wells in an optical lattice is too small to resolve the localized density distri-

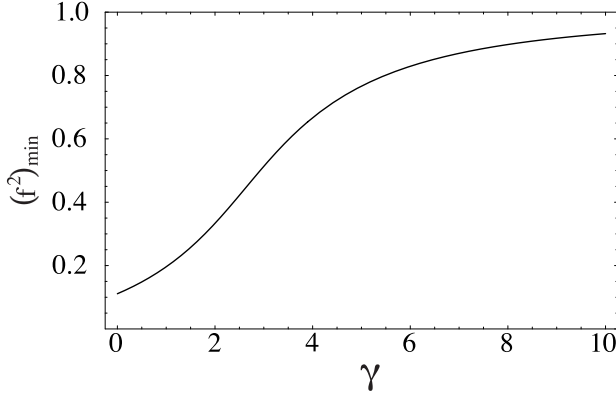


FIG. 2: Minimum value of f^2 during an oscillation period as a function of γ . As γ increases the population imbalance between wells increases (see text).

butions of atoms in neighboring sites using standard imaging techniques.

The momentum distribution is a more convenient observable which approximately corresponds to the expanded spatial distribution of the released condensate. Here we calculate the momentum dynamics of the condensate loaded into every third site of an optical lattice, and show how this relates to evolution of the spatial amplitudes given in Eqs. (16) and (17).

In the tight binding approximation the condensate order parameter $\Phi(x, \tau)$ is expressed as a sum over the lattice sites (2). Because of the periodicity of the system, the momentum space wavefunction, which we denote as $\tilde{\Phi}(k, \tau)$, is expressible as the Fourier series

$$\tilde{\Phi}(k, \tau) = \sum_m \Psi_m(\tau) e^{-ikam} \chi(k), \quad (20)$$

where

$$\chi(k) = \frac{1}{\sqrt{2\pi}} \int_{-\infty}^{\infty} e^{-ikx} \phi_0(x) dx. \quad (21)$$

To compute the momentum distribution, we invoke the identity $\sum_{n=0}^{N_s-1} e^{ikna} = N_s \delta_{k, 2\pi m/a}$, where N_s is the number of lattice sites, and m an integer. Since there are only two independent amplitudes in the set $\{\Psi_m\}$, we find that

$$\begin{aligned} \tilde{\Phi}(k, \tau) &= \sqrt{3/\rho} c_m(\tau) \chi_m \delta_{k, qm/3}, \\ \chi_m &= \chi(qm/3), \\ c_m(\tau) &= \sqrt{\frac{1}{3\rho}} \left(\Psi_0 + \Psi_1 e^{-iqm/3} + \Psi_2 e^{-i2qm/3} \right), \end{aligned} \quad (22)$$

where q is the reciprocal lattice vector $q = 2\pi/a$. The momentum distribution of the system has very sharp peaks of relative amplitude $|c_m|^2$ at momentum $k = qm/3$, arising from the 3-lattice site spatial periodicity of the condensate wavefunction. In addition, χ_m describes a slowly varying envelope determined by the localization of the Wannier states at each lattice site.

Using the analytic solutions for f and g , and Eq. (15), we obtain only two independent Fourier amplitudes

$$|c_{3n}(\tau)|^2 = \frac{1}{3} \left(1 + \frac{\gamma}{4} (3f^2 + 1)(f^2 - 1) \right), \quad (23)$$

$$\begin{aligned} |c_{3n+1}(\tau)|^2 &= \frac{1}{3} \left(1 - \frac{\gamma}{8} (3f^2 + 1)(f^2 - 1) \right) \\ &= |c_{3n+2}(\tau)|^2 \end{aligned} \quad (24)$$

In the reduced zone scheme, where we only consider momenta in the range $k \in [-q/2, q/2]$, the momentum wavefunction then consists of three peaks corresponding to Bloch states of quasimomenta $0, \pm q/3$. The identical behavior of $|c_{3n+1}|^2$ and $|c_{3n+2}|^2$ means that the $\pm q/3$ peaks always have the same intensity. If interactions between the atoms are ignored (i.e. $\gamma = 0$), the momentum components are constant in time (see Eqs. (23) and (24)), even though tunneling occurs between the lattice sites. However, when interactions are considered, the momentum intensities explicitly depend on the occupations of each site and will vary in time when tunneling occurs. The magnitude of the time variation of the $|c_n|^2$ is proportional to γ , but will reduce for sufficiently large values of γ , where the self-trapping effect causes the tunneling between lattice sites to stop (i.e. $f^2 \approx 1$ at all times). In Fig. 3 we show the maximum contrast between the intensity of the Fourier peaks, defined as $\Delta_{\max} \equiv (|c_1|^2 - |c_0|^2)_{\max}$, where the value is maximized by evaluating the $|c_n|^2$ at the time when f takes its minimum value (we note that $f(\tau)$ is given by Eq. (16)). We note that the maximum contrast occurs for $\gamma \approx 3.9$; in this case, the zero quasi-momentum component $c_0(\tau)$ vanishes once during each period of oscillation $T(\gamma)$. For values of γ greater than 3.9 the contrast between the intensities starts to decrease due to the reduction in tunneling caused by the nonlinearity-induced self-trapping.

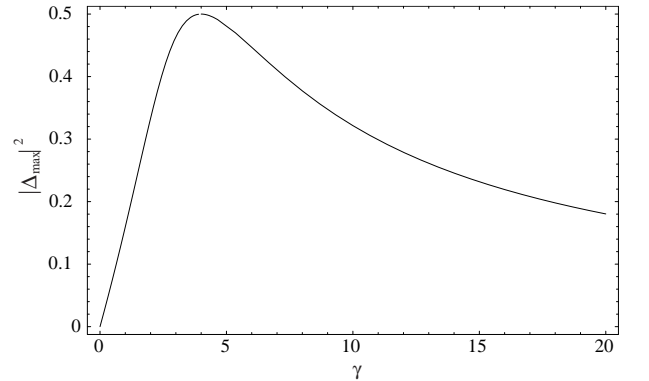


FIG. 3: Maximum contrast of the Fourier components as a function of γ . The maximum contrast is defined as $\Delta_{\max} \equiv (|c_1|^2 - |c_0|^2)_{\max}$ with the maximum value occurring when f^2 is at its minima.

D. Application to an inhomogeneous condensate

Here we wish to consider the dynamics for an inhomogeneous condensate, applicable to a condensate initially pre-

pared in a harmonic trap. For the pattern loaded condensate, we use inhomogeneous to refer to the overall spatial envelope of the period three initial condition. The previous homogeneous theory we have presented is expected to accurately describe inhomogeneous cases when the initial pattern of population in every third site extends over many lattice sites i.e. $N_s \gg 1$ so that mean-field energy associated with each triplet of sites $U(n) = \frac{\Lambda}{2} \sum_{i=1}^3 |\Psi_{3n+i}|^4$ varies slowly across the system. Taking as a particular example we choose a gaussian envelope to the periodic arrangement of atoms into every third site, so that the initial state is

$$\Psi_{3n+1}(0) = \Psi_{3n+2}(0) = 0, \quad (26)$$

$$\Psi_{3n}(0) = 3 \left[\frac{2}{\pi N_s^2} \right]^{1/4} \exp(-(9n/N_s)^2). \quad (27)$$

For the simulations shown here, the parameters used were $N = 10^5$, $N_s = 76$, $U = 2.11 \times 10^{-5} E_R$ and $J = 0.075 E_R$, where $E_R = \hbar^2/8Ma^2$ is the lattice recoil energy; these correspond to a condensate of 10^5 atoms of ^{87}Rb produced in a magnetic trap with axial and radial frequencies of 9 and 12 Hz respectively, and loaded into a lattice of counter-propagating light 785nm of depth $4.5 E_R$, with $E_R = 2.2\text{kHz}$. These parameters are typical of the experimental regime, but also lie in a range in which the homogeneous model is expected to give a fair description. The total number of occupied wells and the strength of the on site interatomic interaction were calculated by preserving the value of chemical potential of the system upon reduction to one spatial dimension and by assuming that each of the localized orbitals in the tight binding description are Gaussian. The hopping rate J was estimated by using Mathieu functions. In Fig. 4 we show the evolution of the population of the central wells (normalized to one) compared with the homogeneous model with γ taken to be the local mean-field energy $\gamma_{\text{eff}} = \Lambda \sqrt{\frac{2}{\pi}} (9/N_s)$.

Figure 4, shows the results of numerical integration of the equations of motion and the approximate analytical solution given by the quasi-homogeneous model described above. We see that the numerical and analytical results agree well at short times, but differ more as time progresses due to the different mean-field seen by different wells.

To understand the disagreement as time evolves, we show in Fig. 5 the numerical Fourier spectrum for the inhomogeneous case evaluated at several different times. The variation of the intensities of the peaks, which, as shown below, is related to the spatial tunneling between lattice sites in the presence of the mean field, can be seen in the plot. Initially all occupied sites are in phase and the three distinctive momentum peaks have a narrow width determined by the intrinsic momentum uncertainty of the condensate envelope. That is the reason why the homogeneous model fits very well. However, as time progresses the meanfield variation across the lattice causes the tunneling rates to vary with position and leads to the momentum peaks broadening. The homogeneous description then, starts not to be very accurate.

We note that momentum space signature for spatially tunneling in the interacting system is still present in the inhomogeneous case. This is shown in Fig. 6, where we plot the

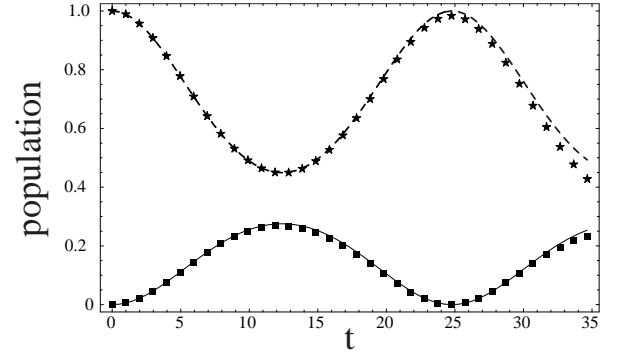


FIG. 4: Comparison between the population evolution of the central three wells for the inhomogeneous condensate and the homogeneous model. inhomogeneous condensate: stars for the initially populated well and boxes for the initial empty wells. Homogeneous model: dashed line represents the initially populated wells, and the solid line represented the initially unpopulated wells. We used γ_{eff} as the local mean field energy. The parameters used for the simulation were $J = 0.075 E_R$ and $\gamma_{\text{eff}} = 2.64$. The time is in computational units: $t \equiv t_{\text{SI}} \hbar / E_R$ where E_R is the recoil energy and t_{SI} is time in SI units. ($10 \hbar / E_R \approx 0.7\text{ms}$).

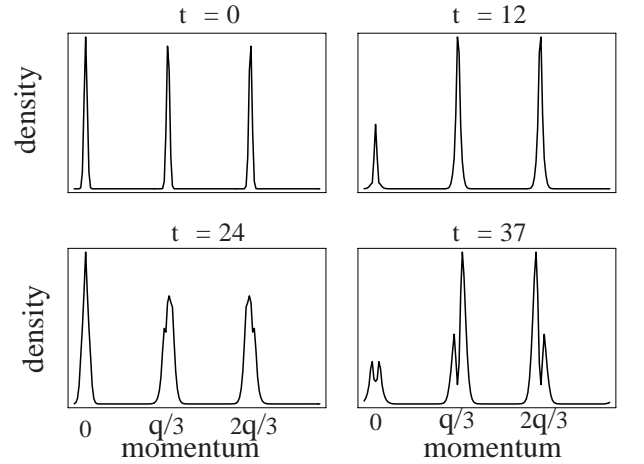


FIG. 5: Momentum distribution of the inhomogeneous condensate evaluated at various times for the same parameters as used in Fig.4.

evolution of the quantities $|c_{3n}(\tau)|^2$, $|c_{3n+1}(\tau)|^2$, $|c_{3n+2}(\tau)|^2$ (calculated from the numerical simulation by partitioning the numerical Fourier spectrum in three equal non overlapping sections, each centered around the respective peak and adding the square of the norm of the Fourier components within each section) vs. the ones calculated with the homogeneous model, but using an averaged value $\gamma_{\text{ave}} \equiv \Lambda \sum_n |\Psi_n|^4$ instead of $\gamma = \Lambda \rho$. It can be observed that the predictions of the simple model are in very good agreement with the numerical results when the three peaks of the spectrum are well defined. For longer times, the width of the Fourier peaks increases, until a point when they split. At this point the quantities $|c_{3n}(\tau)|^2$, $|c_{3n+1}(\tau)|^2$, $|c_{3n+2}(\tau)|^2$ are not meaningful anymore. Because the parameters used for the numerical calculations were

chosen to be experimentally achievable, and as shown in the plots the model predictions are fair at least for one period of oscillation, we conclude that Fourier distribution can be used as a signature of the mean-field quantum tunneling inhibition.

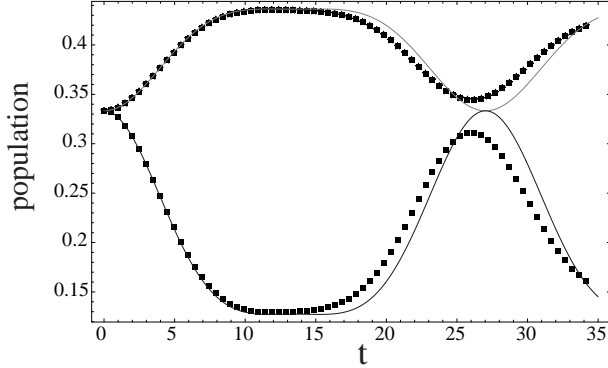


FIG. 6: Evolution of momentum peak populations. Upper curves: population of the $q = \pm 2\pi/3$ momentum states. Lower curves: population of the $q = 0$ momentum state. Inhomogeneous condensate (dotted), homogeneous result (solid line), where the comparison is made by replacing γ by an average mean field energy $\gamma_{\text{ave}} \equiv \Lambda \sum_n |\Psi_n|^4 = 1.85$. Parameters are the same as in Fig. 4.

IV. DYNAMICS WITH A CONSTANT EXTERNAL FORCE

A. Homogeneous three state model

In this section we consider the dynamics of a periodically loaded condensate in the presence of a linear external potential, corresponding to a uniform force parallel to the lattice. In what follows we assume that the force is sufficiently weak that band excitations due to Landau-Zener tunneling is negligible, so that a tight binding picture of the lowest band is sufficient to describe the dynamics. In this case the evolution equation differs from what we considered in the previous section by the term E_n in Eq. (5) taking the form $E_n = n\xi$, where ξ is the potential difference between lattice sites (in units of the hopping matrix element J). Taking the initial conditions (6)-(7), and transforming the Wannier amplitudes as $\Psi_{3n+j}(\tau) = \tilde{\Psi}_{3n+j}(\tau)e^{-i3n\xi\tau}$ ($j = 0, 1, 2$), we obtain the evolution equations

$$i\frac{\partial \tilde{\Psi}_{3n}}{\partial \tau} = -(\tilde{\Psi}_{3n-1}e^{i3\xi\tau} + \tilde{\Psi}_{3n+1}) + \Lambda|\tilde{\Psi}_{3n}|^2\tilde{\Psi}_{3n}, \quad (28)$$

$$i\frac{\partial \tilde{\Psi}_{3n+1}}{\partial \tau} = -(\tilde{\Psi}_{3n+2} + \tilde{\Psi}_{3n}) + \xi\tilde{\Psi}_{3n+1} + \Lambda|\tilde{\Psi}_{3n+1}|^2\tilde{\Psi}_{3n+1}, \quad (29)$$

$$i\frac{\partial \tilde{\Psi}_{3n+2}}{\partial \tau} = -(\tilde{\Psi}_{3n+1} + \tilde{\Psi}_{3n+3}e^{-i3\xi\tau}) + 2\xi\tilde{\Psi}_{3n+1} + \Lambda|\tilde{\Psi}_{3n+1}|^2\tilde{\Psi}_{3n+1}, \quad (30)$$

Assuming periodic boundary conditions, the periodicity of the initial conditions and equations of evolution allow considerable simplification from the full set of $3T$ coupled equations. In particular these assumptions mean that every third Wannier amplitude evolves identically (i.e. $\tilde{\Psi}_n = \tilde{\Psi}_{n+3}$) and so the evolution of the system can hence be reduced to the three independent equations

$$i\frac{\partial \tilde{\Psi}_0}{\partial \tau} = -(\tilde{\Psi}_2e^{i3\xi\tau} + \tilde{\Psi}_1) + \Lambda|\tilde{\Psi}_0|^2\tilde{\Psi}_0, \quad (31)$$

$$i\frac{\partial \tilde{\Psi}_1}{\partial \tau} = -(\tilde{\Psi}_2 + \tilde{\Psi}_0) + \xi\tilde{\Psi}_1 + \Lambda|\tilde{\Psi}_1|^2\tilde{\Psi}_1, \quad (32)$$

$$i\frac{\partial \tilde{\Psi}_2}{\partial \tau} = -(\tilde{\Psi}_1 + \tilde{\Psi}_0e^{-i3\xi\tau}) + 2\xi\tilde{\Psi}_2 + \Lambda|\tilde{\Psi}_2|^2\tilde{\Psi}_2, \quad (33)$$

where the new amplitudes map onto the original set according to $\tilde{\Psi}_0 \leftrightarrow \{\tilde{\Psi}_{3n}\}$, $\tilde{\Psi}_1 \leftrightarrow \{\tilde{\Psi}_{3n+1}\}$, and $\tilde{\Psi}_2 \leftrightarrow \{\tilde{\Psi}_{3n+2}\}$, and obey the normalization condition

$$\sum_{j=0}^2 |\tilde{\Psi}_j|^2 = \frac{1}{T}. \quad (34)$$

The equations of motion (31)-(33) are more difficult to treat analytically than the case considered in the last section due to the presence of a linear potential. In this paper we derive an analytic solution for a noninteracting condensate (i.e. $\Lambda=0$), which provides valuable insight into the complicated tunneling dynamics the system exhibits in the absence of nonlinearity, yet should furnish a good description for dilute condensates satisfying $\gamma \ll 1$. For the nonlinear regime we present numerical results to illustrate typical behavior.

B. Analytic solution for linear dynamics

Defining the vector $\mathbf{x}(t) = (\tilde{\Psi}_0(\tau), \tilde{\Psi}_1(\tau), \tilde{\Psi}_2(\tau))$, and using the transformation $\mathbf{y}(\tau) = P(\tau)\mathbf{x}(\tau)$, where $P(\tau)$ is the unitary matrix

$$P(\tau) = \begin{pmatrix} 1 & 1 & 1 \\ e^{-i\xi\tau} & e^{-i(\xi\tau - \frac{2\pi}{3})} & e^{-i(\xi\tau + \frac{2\pi}{3})} \\ e^{-i2\xi\tau} & e^{-i(2\xi\tau + \frac{2\pi}{3})} & e^{-i(2\xi\tau - \frac{2\pi}{3})} \end{pmatrix}, \quad (35)$$

the linear version of Eqs. (31)-(33) can be decoupled, directly yielding the solutions

$$\tilde{\Psi}_n(\tau) = \frac{e^{-in\xi\tau}}{3\sqrt{T}} \left(e^{-i\Delta_0(\tau)} + e^{i(\frac{2n\pi}{3} - \Delta_1(\tau))} + e^{-i(\frac{2n\pi}{3} + \Delta_2(\tau))} \right), \quad (36)$$

where we have defined the phase terms

$$\Delta_n(\tau) = -\frac{2}{\xi} \left[\sin(\xi\tau - \frac{2n\pi}{3}) + \sin(\frac{2n\pi}{3}) \right] \quad (37)$$

for $n = 0, 1, 2$.

These solutions for the spatial amplitudes $\tilde{\Psi}_i(\tau)$ can be most easily understood by considering a Bloch state decomposition of the condensate wavefunction. The nature of our system allows us to construct an analytic form for the initial wavefunction. Because the system has a three lattice site period and is assumed to be in the lowest band, the wavefunction can be expressed as a superposition of three Bloch waves (of the lowest band) which are symmetrically spaced in quasimomentum. Assuming the condensate initially has a total crystal momentum of zero, at this time the wavefunction must be of the form

$$\Phi(x, 0) = \alpha_0 \varphi_0(x) + \alpha_+ \varphi_{q/3}(x) + \alpha_- \varphi_{-q/3}(x) \quad (38)$$

where $\varphi_k(x)$ is a Bloch state with quasimomentum k , and the α are complex constants determined by the lattice depth, with $|\alpha_+| = |\alpha_-|$.

The action of an external force on a Bloch state causes it to linearly change its quasimomentum in time according to

$$k(\tau) = -\frac{\xi}{a}\tau + k(0). \quad (39)$$

The periodicity of the Bloch dispersion relation in k , and hence of the group velocity of the Bloch wave, gives rise to the well-known phenomenon of Bloch oscillations [29]. For the case we are considering here, the system consists of three Bloch states whose quasimomenta will translate in unison under the action of the external force. During this evolution each state accumulates phase at a rate determined by the instantaneous Bloch energy, i.e.

$$\Delta_n(\tau) = \int_0^\tau E(k_n(s))ds, \quad (40)$$

where $k_n(\tau) = -\xi\tau/a + k_n(0)$ is the quasimomentum of Bloch state n at time t . In the tight binding approximation the dispersion relation for the Bloch states has the analytic form

$$E(k) = -2 \cos(ka), \quad (41)$$

for which $\Delta_n(\tau)$ can be evaluated, and yields the results given in Eqs. (37)). The wavefunction evolution in the Bloch basis is

$$\begin{aligned} \Phi(x, \tau) = & \alpha_0 \varphi_{-\frac{\xi}{a}\tau}(x) e^{-i\Delta_0(\tau)} + \alpha_+ \varphi_{-\frac{\xi}{a}\tau + \frac{q}{3}}(x) e^{-i\Delta_1(\tau)} \\ & + \alpha_- \varphi_{-\frac{\xi}{a}\tau - \frac{q}{3}}(x) e^{-i\Delta_2(\tau)}. \end{aligned} \quad (42)$$

From this solution we can obtain solutions for the evolution of the spatial amplitudes Eqs. (37). To do this we expand the Bloch states in terms of Wannier functions according to $\varphi_{nk}(x) = \sum_n e^{ikna} \phi_n(x)$ and make use of Eq. (2). Note: we take all $\alpha = \frac{\rho}{3}$ as determined by the initial conditions, Eqs.(6) and (7).

1. Bloch Oscillations

The evolution of the spatial amplitudes, and in particular the population in each well is then determined by the interference

of the Bloch phases Δ_n . These functions are all periodic in time with period $\tau_B = 2\pi/\xi$ (in units of $\tau = tJ/\hbar$). This is the normal Bloch oscillation period, and gives the time scale over which the quasimomenta of the Bloch states develop by exactly a lattice vector.

2. Small ξ solution - Non classical transport

To understand the dynamics, we first start by considering the case when ξ is small. For this case, the population in the wells is given by

$$|\tilde{\Psi}_0(\tau)|^2 = \frac{1}{3N_s} \left(5 + 4 \cos(3\tau) + \xi^2 h(\tau) \right) \quad (43)$$

$$|\tilde{\Psi}_1(\tau)|^2 = \frac{1}{3N_s} \left((2 + 3\xi)[1 - \cos(3\tau) - \frac{\xi^2}{2} h(\tau)] \right) \quad (44)$$

$$|\tilde{\Psi}_2(\tau)|^2 = \frac{1}{3N_s} \left((2 - 3\xi)[1 - \cos(3\tau) - \frac{\xi^2}{2} h(\tau)] \right) \quad (45)$$

where

$$h(\tau) = \frac{\tau^3}{2} (6\tau + 3\tau \cos(3\tau) - 4 \sin(3\tau)). \quad (46)$$

The above solution shows that when the force is applied, the degeneracy in the population of the wells represented by $\tilde{\Psi}_1$ and $\tilde{\Psi}_2$ is lifted. For $\xi > 0$, atoms in $\tilde{\Psi}_0$ start to tunnel to $\tilde{\Psi}_1$ more rapidly than to $\tilde{\Psi}_2$. This should be compared with the results in the absence of the force, where $\tilde{\Psi}_1$ and $\tilde{\Psi}_2$ behave identically. Thus, in this weak limit, the effect of a linear potential to enhance the tunneling from the initial populated $3n$ wells to their $3n + 1$ neighbors ones, making the system closer to resonance, in the sense of Eq. (12), where the resonance condition results in the initially populated wells becoming empty at some later time. It is interesting to note that the system exhibits "nonclassical" dynamics whereby the atoms start to tunnel in the direction opposite the direction of the force (this statement applies even when the external field is not weak).

3. Resonances

In Fig. 7 we show the temporal evolution of the spatial amplitudes $\tilde{\Psi}_i$ for a range of values of ξ . For certain choices of ξ the initially occupied $\tilde{\Psi}_0$ amplitude periodically disappears - we refer to these as resonances. By requiring $\tilde{\Psi}_0 = 0$ in Eq. (36) we obtain the following conditions on the phases for these resonances

$$\Delta_1(\tau) - \Delta_0(\tau) = \pm \left(\frac{\pi}{3} + 2\pi n \right) \quad (47)$$

$$\Delta_2(\tau) - \Delta_1(\tau) = \pm \left(\frac{\pi}{3} + 2\pi m \right) \quad (48)$$

where n and m are integers and the same sign choice on the right hand side must be made for both equations. When these conditions are satisfied the population is not shared between the adjacent sites, but preferentially tunnels to one of

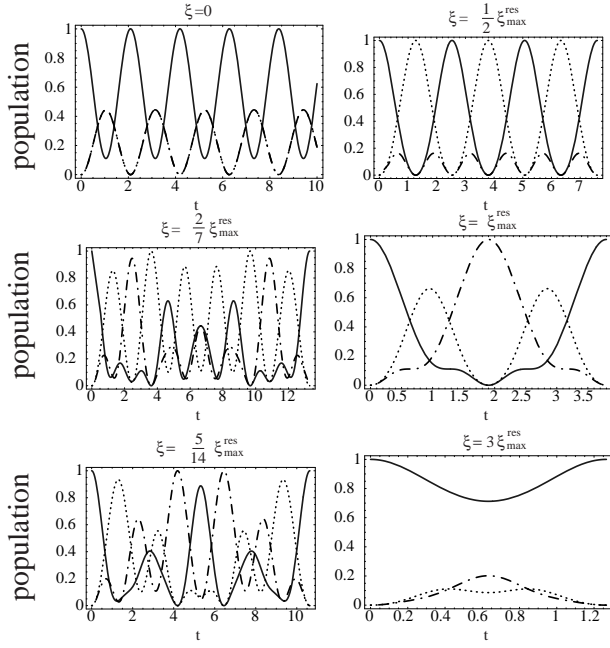


FIG. 7: Evolution of the normalized population for different values of ξ . One Bloch period is shown in the plots except $\xi = 0$ where the period is infinite. Solid line: $|\Psi_{3n}|^2$, dotted line: $|\Psi_{3n+1}|^2$, dashed line: $|\Psi_{3n+2}|^2$. The “nonclassical” motion can be seen where the $3n+1$ -well populations increase more rapidly than the populations of the $3n+2$ -wells. It can also be seen in the plots that $\xi = \xi_{\max}/2$ and $\xi = \xi_{\max}$ are resonant values.

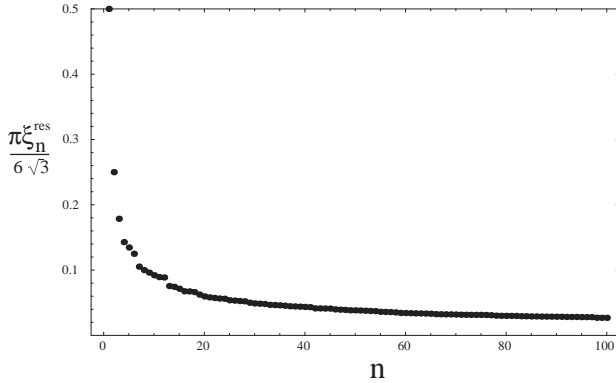


FIG. 8: The spectrum of values of external force, ordered in decreasing magnitude, for which a population resonance occurs i.e. the values of ξ for which $\tilde{\Psi}_0$ periodically disappears

the neighbors. In particular the $+$ sign choice in Eqs. (47) and (48), gives the phase condition for complete tunneling into $\tilde{\Psi}_1$. Similarly the $-$ sign case gives the condition for complete tunneling into $\tilde{\Psi}_2$. Solving for the values of ξ for which Eqs. (47) and (48) hold, gives the spectrum

$$\xi_{nm}^{\text{res}} = \pm \frac{6\sqrt{3}}{\pi} \frac{(1+3n)}{(1+3n)^2 + 3(n+2m+1)^2}. \quad (49)$$

which is shown in Fig. 8. For large $|n|$ or $|m|$ the resonant values of ξ are close together, and become spaced further apart as the magnitude of n decreases.

In the absence of an applied force (i.e. $\xi = 0$) the phase terms are time-independent with $\Delta_0 = -2$, $\Delta_1 = -1$ and $\Delta_2 = -1$ so that the resonance conditions can never be achieved. When the external force is applied the phases oscillate at a rate that increases with ξ and an amplitude that decreases with ξ . The largest value of ξ for which a resonance can be found is $\xi_{\max}^{\text{res}} \equiv 6\sqrt{3}/2\pi$, since for values of ξ greater than this the amplitudes of the phase oscillations Δ_i are so small that they cannot satisfy the condition for population resonance. In the regime $\xi > \xi_{\max}^{\text{res}}$, $|\tilde{\Psi}_0|$ exhibits only one (nonzero) minima per Bloch period and the dynamics of the system is dominated by the Bloch oscillations.

4. Large Force Limit

For $\xi > \xi_{\max}^{\text{res}}$ the system exhibits a population imbalance as the Bloch oscillation suppresses the ability of the system to tunnel between sites. In the limit $\xi \gg \xi_{\max}^{\text{res}}$ the population in the wells is described by rapid, small amplitude oscillations around its initial value,

$$|\tilde{\Psi}_0(\tau)|^2 \rightarrow \frac{3}{N_s} \left(1 - \frac{8}{\xi^2} \sin^2 \left(\frac{\xi\tau}{2} \right) \right) \quad (50)$$

$$|\tilde{\Psi}_1(\tau)|^2 \rightarrow \frac{12}{N_s} \frac{1}{\xi^2} \sin^2 \left(\frac{\xi\tau}{2} \right) \quad (51)$$

$$|\tilde{\Psi}_2(\tau)|^2 \rightarrow \frac{12}{N_s} \frac{1}{\xi^2} \sin^2 \left(\frac{\xi\tau}{2} \right) \quad (52)$$

The case of $\xi = 3\xi_{\max}^{\text{res}}$ depicted in Fig. 8 shows an approach to this behavior.

C. Numerical results for the non-linear case

Because of the difficulty of solving analytically the equations of motion the nonlinear equations were solved numerically. Although the dynamics in this situation is considerably more complicated than in the linear case, the resonance picture still gives us useful guidance concerning the expected behavior. In general, there exist critical values of ξ and Λ above which no resonances occur. Furthermore, nonlinearity tends to destroy the periodicity of the Bloch oscillations that is present in the noninteracting case. For example, in Fig. 9, we see that for $\xi = 2\xi_{\max}^{\text{res}}$, the introduction of interactions brings the system into resonance, but that for large interaction strength, nonresonant behavior is restored. For $\xi = 2\xi_{\max}^{\text{res}}/7$, on the other hand, the introduction of interactions eventually draws the system out of resonance.

Concerning the momentum distribution, similarly to the un-tilted case, interatomic interactions induce time variation of the momentum intensities. The contrast between momentum components vanishes at $\Lambda = 0$. As Λ increases, the contrast

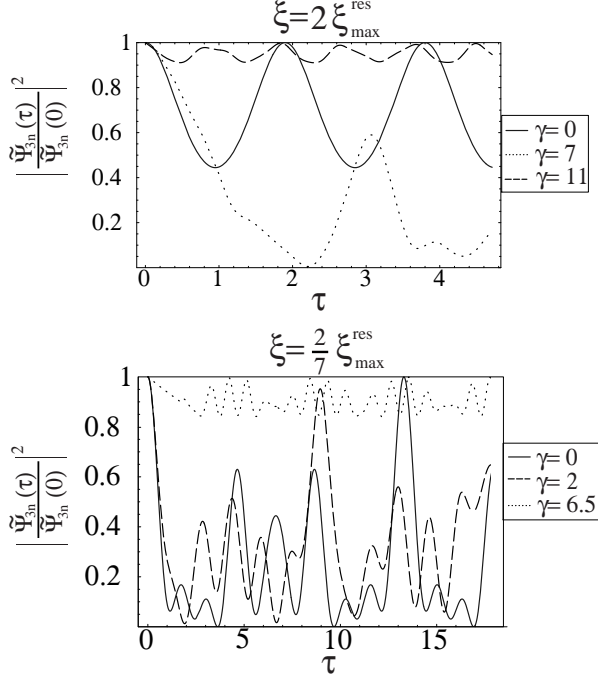


FIG. 9: Effects of interactions on generalized Bloch oscillations for the pattern loaded system. Evolution of $|\tilde{\Psi}_n|^2$ for various interaction strengths. Upper plot: $\xi = 2\xi_{\max}^{\text{res}}$. Lower plot: $\xi = 2\xi_{\max}^{\text{res}}/7$.

increases to a maximum value, then eventually decreases towards zero when macroscopic imbalance is achieved, analogous to what is seen in Fig. 3 for the untilted case. Because the external field together with the nonlinearity breaks down the periodicity of time evolution, the dynamics of the momentum distribution is quite complex.

To compare the predictions of the homogeneous model in the presence of a linear external potential to a more realistic case, we again solved numerically the discrete nonlinear Schrödinger equation for a condensate loaded every three lattice sites but, instead of being homogeneous, initially with a Gaussian profile. Very good agreement between the model and the numerical results was found for short times and modest mean-field energies, if, as in the untilted case, we use an effective mean field energy. In Figs. 10 and 11 we present a comparison between the evolution of the normalized population at the central wells found numerically and the prediction of the model for the parameters: $NU = 4.8E_R$, $N_s = 290$, $J = 0.075E_R$ and $\xi = 2$ with computational time of 50 is about 3.5 ms. For longer times, the model predictions start to disagree with numerical simulation due to the spread of the three Fourier peaks. We observe that the dynamics are much more sensitive to inhomogeneous effects in the presence of an external force, and for the more inhomogeneous initial state used in Figs. 4-6 (which extends over $N_s = 76$ sites), the inhomogeneous result much more rapidly departs from the homogeneous prediction than the example presented here.

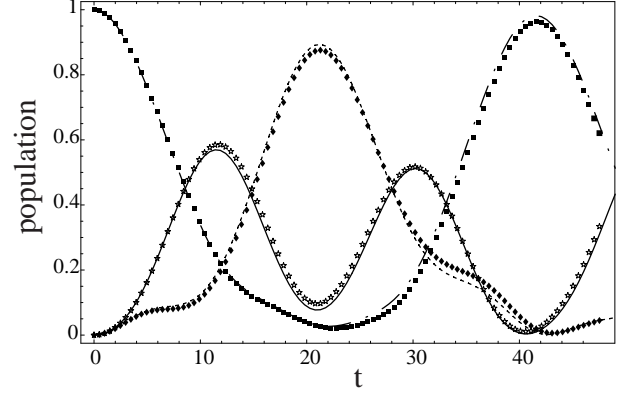


FIG. 10: Comparison between the evolution of an inhomogeneous condensate with the homogeneous result. Inhomogeneous condensate: $|\tilde{\Psi}_0|^2$ (boxes), $|\tilde{\Psi}_1|^2$ (stars), and $|\tilde{\Psi}_2|^2$ (diamonds). Homogeneous case: $|\tilde{\Psi}_{3n}|^2$ (dash-dot line), $|\tilde{\Psi}_{3n+1}|^2$ (solid line), and $|\tilde{\Psi}_{3n+2}|^2$ (dotted line), where we have taken γ as the local mean field energy. The parameters used were $J = 0.075E_R$, $\xi = 2$ and $\gamma_{\text{eff}} = 1.59$.

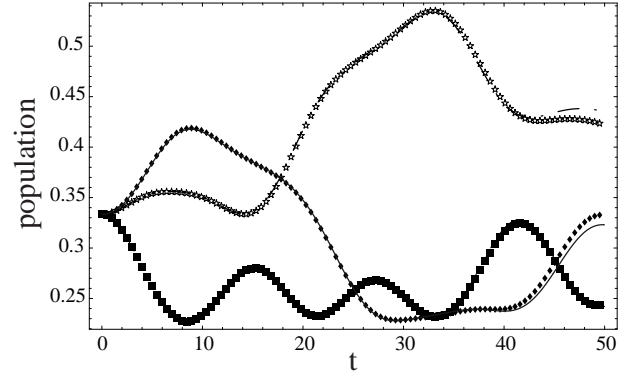


FIG. 11: Evolution of the momentum peak populations. $q = 0$ (dashed line, squares), $q = -2\pi/3$ (dash-dot line, stars), $q = 2\pi/3$ (solid line, diamonds). Inhomogeneous condensate (dotted curves), homogeneous model (lines) using the same parameters as those in Fig. 10, but replacing γ by an average value $\gamma_{\text{ave}} = 1.11$ for the homogeneous model.

V. CONCLUSION

We have studied the dynamics of a condensate loaded in an optical lattice in such a way that initially only every third well in the lattice was occupied. We considered two cases, one with only the optical potential, and one with a superimposed constant external field. It was found that in both cases interatomic interactions can cause macroscopic quantum self trapping, which is a self maintained population imbalance across the wells. The analysis was based on a tight binding model that assumes that at $\tau = 0$ all the $3n$ wells were identically populated. Using this model, we studied the different regimes where the self trapping phenomenon occurs and estimated the critical parameters for each case. We have developed an analytic solution for the dynamics of a periodic initial condition in

the absence of an external potential. For this case the symmetry of the system reduces the discrete nonlinear Schrödinger equation to a two-mode problem with an elliptic function solution. We have verified the usefulness of the analytic solution by comparing it to numerical solutions of the discrete nonlinear Schrödinger equation for more general initial conditions.

We have demonstrated that meanfield effects cause the momentum distribution to vary with time, and have shown how this variation relates to the spatial tunneling in the system. This result suggests that the temporal variation in the time-of-flight density distribution (which approximately corresponds to the *in-situ* momentum distribution) would be a useful experimental signature of the spatial tunneling.

In the presence of an external potential and neglecting interactions, it was found that the spatial population amplitudes

evolve periodically in time, with the oscillation period determined by the force parameter ξ . We have shown that these dynamics can be understood as the interference of three quasi-momentum states Bloch oscillating in unison. When interactions are taken into account, the periodicity of the system is destroyed and the atoms exhibit more complicated dynamics.

Acknowledgements

This work was supported in part by the Advanced Research and Development Activity and by the U.S. National Science Foundation under grant PHY-0100767.

-
- [1] B. Anderson and M. Kasevich, *Science* **282**, 1686 (1998).
 - [2] M. Greiner, I. Bloch, O. Mandel, T. W. Hansch, and T. Esslinger, *Phys. Rev. Lett.* **87**, 160405 (2001).
 - [3] J. H. Denschlag, J. E. Simsarian, H. Häffner, C. McKenzie, A. Browaeys, D. Cho, K. Helmerson, S. L. Rolston, and W. D. Phillips, *J. Phys. B* **35**, 3095 (2002).
 - [4] W. K. Hensinger, H. Häffner, A. Browaeys, N. R. Heckenberg, K. Helmerson, C. McKenzie, G. J. Milburn, W. D. Phillips, S. L. Rolston, H. Rubinsztein-Dunlop, et al., *Nature* **412**, 52 (2001).
 - [5] O. Morsch, J. H. Muller, M. Cristiani, D. Ciampini, and E. Arimondo, *Phys. Rev. Lett.* **87**, 140402 (2001).
 - [6] S. Burger, F. S. Cataliotti, C. Fort, F. Minardi, M. Inguscio, M. L. Chiofalo, and M. P. Tosi, *Phys. Rev. Lett.* **86**, 4447 (2001).
 - [7] O. Morsch, M. Cristiani, J. H. Muller, D. Ciampini, and E. Arimondo, *Phys. Rev. A* **66**, 021601 (2002).
 - [8] C. Orzel, A. K. Tuchman, M. L. Fenselau, M. Yasuda, and M. A. Kasevich, *Science* **23**, 2386 (2001).
 - [9] M. Greiner, O. Mandel, T. Esslinger, T. W. Hansch, and I. Bloch, *Nature* **415**, 39 (2002).
 - [10] S. Peil, J. V. Porto, B. L. Tolra, J. M. Orecht, B. E. King, M. Subbotin, S. L. Rolston, and W. D. Phillips, *in preparation*.
 - [11] A.-M. Rey and *et al.*, *In preparation* (2002).
 - [12] D. I. Choi and Q. Niu, *Phys. Rev. Lett.* **82**, 2022 (1999).
 - [13] J. C. Bronski, L. D. Carr, B. Deconinck, and J. N. Kutz, *Phys. Rev. Lett.* **86**, 1402 (2001).
 - [14] S. Raghavan, A. Smerzi, S. Fantoni, and S. R. Shenoy, *Phys. Rev. A* **59**, 620 (1999).
 - [15] I. Marino, S. Raghavan, S. Fantoni, S. R. Shenoy, and A. Smerzi, *Phys. Rev. A* **60**, 487 (1999).
 - [16] S. Raghavan, A. Smerzi, and V. M. Kenkre, *Phys. Rev. A* **60**, 1787 (1999).
 - [17] A. Smerzi and S. Raghavan, *Phys. Rev. A* **61**, 063601 (2000).
 - [18] S. Giovanazzi, A. Smerzi, and S. Fantoni, *Phys. Rev. Lett.* **84**, 4521 (2000).
 - [19] M. BenDahan, E. Peik, J. Reichel, Y. Castin, and C. Salomon, *Phys. Rev. Lett.* **76**, 4508 (1996).
 - [20] M. L. Chiofalo and M. P. Tosi, *Phys. Lett. A* **268**, 406 (2000).
 - [21] J. M. Ziman, *Principles of the Theory of Solids* (Cambridge at the University Press, 1964).
 - [22] A. Trombettoni and A. Smerzi, *J. Phys. B* **34**, 4711 (2001).
 - [23] A. Trombettoni and A. Smerzi, *Phys. Rev. Lett.* **86**, 2353 (2001).
 - [24] B. Wu, R. B. Diener, and Q. Niu, *Phys. Rev. A* **65**, 025601 (2002).
 - [25] G. J. Milburn, J. Corney, E. M. Wright, and D. F. Walls, *Phys. Rev. A* **55**, 4318 (1997).
 - [26] A. Smerzi, S. Fantoni, S. Giovanazzi, and S. R. Shenoy, *Phys. Rev. Lett.* **79**, 4950 (1997).
 - [27] I. Abramowitz and I. A. Stegun, *Handbook of Mathematical Functions* (National Bureau of Standards, 1964).
 - [28] C. Cohen-Tannoudji, B. Diu, and F. Laloë, *Quantum Mechanics*, vol. 2 (John Wiley and Sons, 1977).
 - [29] N. W. Ashcroft and N. D. Mermin, *Solid State Physics* (W.B. Saunders Company, 1976).